The structural dynamics in the proton-conducting imidazolium oxalate

2008 J. Phys.: Condens. Matter 20 505101

(http://iopscience.iop.org/0953-8984/20/50/505101)

J. Phys.: Condens. Matter **20** (2008) 505101 (7pp) doi:10.1088/0953-8984/20/50/505101

The structural dynamics in the proton-conducting imidazolium oxalate

Adam Rachocki[1], Katarzyna Pogorzelec-Glaser[1], Adam Pietraszko[2] and Jadwiga Tritt-Goc[1]

[1] Institute of Molecular Physics, Polish Academy of Sciences, M. Smoluchowskiego 17, 60-179 Poznań, Poland
[2] Institute of Low Temperature and Structure Research, Polish Academy of Sciences, Okólna 2, 50-422 Wrocław, Poland

E-mail: radam@ifmpan.poznan.pl

Received 16 August 2008, in final form 28 September 2008
Published 7 November 2008
Online at stacks.iop.org/JPhysCM/20/505101

Abstract
The ^{1}H spin–lattice relaxation times and high-resolution solid-state nuclear magnetic resonance (NMR) under fast magic spinning were used to study the structural dynamics in the proton-conducting material imidazolium oxalate. The measurements provide evidence for the ordered and disordered domains within the studied material. The two components drastically differ in their ^{1}H spin–lattice relaxation times and ^{1}H–^{13}C cross-polarization magic-angle-spinning (CP/MAS) spectra. The coalescence phenomenon of the resonances of the basal carbons of the imidazole ring undergoing a reorientation is observed only for mobile molecules in the disordered domains. Therefore, only these molecules can be responsible for proton conductivity allowing for the Grotthus mechanism.

(Some figures in this article are in colour only in the electronic version)

1. Introduction

The imidazolium salts of dicarboxylic acids form a new class of imidazole-based proton conductors, which were aimed at generating improved membranes for fuel cells. They represent water-free materials and thanks to this fuel cells with imidazolium salts of dicarboxylic acids, used as solid electrolyte membranes, could operate at intermediate temperature (above 100 °C). The first time some imidazolium salts of monocarboxylic and dicarboxylic acids were designed and synthesized was by MacDonald *et al* [1]. They also solved their crystal structures. The characteristic features of these structures are the polar hydrogen-bonded layers formed by the imidazolium salts of dicarboxylic acids composed of intersections of chains of N–H $\cdots$ O and O–H $\cdots$ O hydrogen bonds. The carboxylic anions serve as acceptors for multiple hydrogen bonds that organize and orient imidazolium cations and carboxylic anions in two dimensions. Imidazolium cations function as hydrogen-bonding donors that cross-link chains of anions. They also form multiple C–H $\cdots$ O hydrogen bonds, which link anions in adjacent layers [1]. The two-dimensional network of the hydrogen bonds in the imidazolium salts of carboxylic acids forms a convenient paths for proton transport in such materials.

In our laboratory new salts, imidazolium malonate, imidazolium gluterate, imidazolium adipate monohydrate, di-imidazolium suberate, imidazolium sebacate and imidazolium succinate, have been synthesized [2, 3]. The electrical conductivity measurements confirmed their proton-conducting properties. The measured values of electrical conductivities are in a similar range of 10^{-5}–10^{-1} S m^{-1} between 368 and 401 K, i.e., just below the respective melting temperatures [2, 3]. The crystal structures of these new salts were also determined [3, 4] and showed the hydrogen-bonded layer structure as in the other imidazolium salts of dicarboxylic acids obtained by MacDonald *et al* [1].

It is well known that the very high proton conductivity of hydrated polymers relies on the presence of liquid water [5, 6]. The substitution of water by heterocycles such as imidazole also leads to high proton conductivities [7, 8] and the transport properties in the liquid state are similar to water [8]. The liquid-like electrolytes are actually most likely used in fuel cell technology. However, the imidazole-based materials in solid state can also serve as proton carriers in membranes for fuel cells. Good candidates beside the imidazolium salts

of dicarboxylic acids are imidazole-terminated ethyleneoxide oligomers [9–12] or imidazolium methyl sulfonate [13]. The measured proton conductivity in imidazole–ethyleneoxides is about 10^{-1} S m^{-1} at 120 °C [9]. In all imidazole-based materials and in imidazole itself the proton mobility relies on structure diffusion (Grotthus-type mechanism), which involves proton transfer between imidazole molecules and their reorganization [14–16]. The solid nuclear magnetic resonance (NMR) studies in imidazolium methyl sulfonate evidence that this reorientation is a fast 180°-flip motion of the imidazole ring [13, 17]. It is believed that the flip motion is the rate-limiting step for proton transport in imidazole-based materials intended for fuel cell applications.

In the studied imidazolium oxalate (imi-oxalate), the arrangement of imidazole molecules and acid chains and their mobilities at different length scales and timescales are the critical factors which influence the proton transport properties. Therefore, to understand and optimize these properties, it is necessary to characterize not only its rigid structure but also structural dynamics. These two subjects were the main goal of our studies presented in this paper. The crystal structure of imi-oxalate was studied by x-ray at 298 K in order to confirm the synthesized material. The structural dynamics were determined thanks to the ^{1}H spin–lattice relaxation and high-resolution solid-state ^{1}H–^{13}C CP/MAS (cross-polarization magic-angle-spinning) NMR (nuclear magnetic resonance) measurements.

From the family of new synthesized imidazolium salts of carboxylic acids the imi-oxalate was chosen for the NMR studies because it has a relatively simple molecular and crystal structure and can serve as a model system for this class of imidazole-based materials. The electrical conductivity of imi-oxalate behaves very similarly to that of the other imidazolium salts of dicarboxylic acids and will be the subject of a separate paper.

2. Experimental details

2.1. Synthesis and crystallization

Imidazole and oxalic acid, the starting materials with a purity of about 99%, were purchased from Sigma-Aldrich and Fluka Company Ltd. They were separately dissolved in anhydrous ethyl acetate and next the mixtures were added together. The reaction product in the form of a white precipitate was separated and washed with anhydrous ethyl acetate. Crystallization of the imi-oxalate was carried out from the acetone solution of the precipitate.

2.2. X-ray measurements

Single-crystal x-ray diffraction measurements were performed using an x-ray four-circle Xcalibur diffractometer (Oxford Diffraction Company) with CCD area detector at 298–330 K. Graphite monochromated Mo Kα radiation was generated at 50 kV and 25 mA. The crystal structure of the studied salt was determined using SHELXL-97 and JANA2000 programs [18, 19]. The calculations of the anharmonic probability density functions (PDFs) were used to analyze the anharmonic motion of atoms of the studied compound [20]. The CIF files with the crystal data at 298 K were sent to a deposit in the Cambridge Structural Database (CSD).

2.3. Proton spin–lattice and ^1H–^{13}C CP/MAS NMR measurements

The sample of polycrystalline imi-oxalate used for the proton-spin–lattice NMR relaxation time (T_1) measurements was stored in a glass tube, evacuated at room temperature at 0.1 Pa for 6 h to remove oxygen and finally sealed under vacuum. The relaxation time T_1 measurements were carried out on a Bruker pulse spectrometer operating at ^{1}H frequencies of 90 MHz in the temperature range from 87 to 440 K. The measurements did not reach the melted phase of imi-oxalate because the melting temperature for this salt was determined to be $T_m = 523$ K [1]. Spin–lattice relaxation times were determined by the saturation-recovery solid-echo technique: $(n \times 90^\circ_x) - \tau - (90^\circ_x - t_{SE} - 90^\circ_y)$. In our experiments the saturation pulse sequence took 75 ms and consumed $n = 25$ of $\pi/2$-pulses with the length set to 4 μs. The solid-echo signals were observed for $t_{SE} = 17$ μs. About 30–40 experimental points of the recovered solid-echo amplitude were acquired from the maximum of the solid-echo shape for τ delay values varying from 1 ms to a few hours. Moreover, there was only one accumulation applied for the longest times τ (order of half an hour and more), when two and four accumulations of data points were used for the shorter τ delay values. The errors in the measurements of T_1 were estimated to be about 5 to a maximum of 10%. The nonexponential recovery of magnetization was found in the whole temperature range. The temperature of the samples was controlled by means of a continuous nitrogen gas-flow system and determined with an accuracy of ±1 K. The relaxation measurements performed for imi-oxalate are very time consuming. This may be the reason that for imidazole-based materials the relaxation measurements are not available in a wide temperature range. Usually, the relaxation time is measured only at room temperature.

^{13}C magic-angle-spinning (MAS) NMR spectra of imi-oxalate with ^{1}H–^{13}C cross-polarization (CP) were performed on a Bruker Avance III spectrometer equipped with a dual-channel broadband MAS probe-head, operating at ^{13}C frequencies of 75.47 MHz. The powdered sample was spun in a 4 mm ZrO_2 rotor at 8 kHz. The field strength for ^{1}H decoupling was 1.05 mT, contact time 2 ms, and spectral width 25 kHz. The spectra were measured at room temperature.

3. Results and discussion

3.1. Crystal structure analysis

Our crystallographic data of imidazolium oxalate ($C_5H_6N_2O_4$) taken at 298 K confirmed the previous results obtained by MacDonald *et al* [1]. The crystal structure belongs to the monoclinic system with $P2_1/n$ space group, with cell parameters of $\beta = 105.63(4)^\circ$, $a = 5.6995(4)$, $b = 17.529(4)$, $c = 6.819(2)$ nm and $V = 655.66(7)$ nm^3. The unit cell contains four molecules. Imidazolium cations and carboxylic anions self-assembled via N–H $\cdots$ O hydrogen

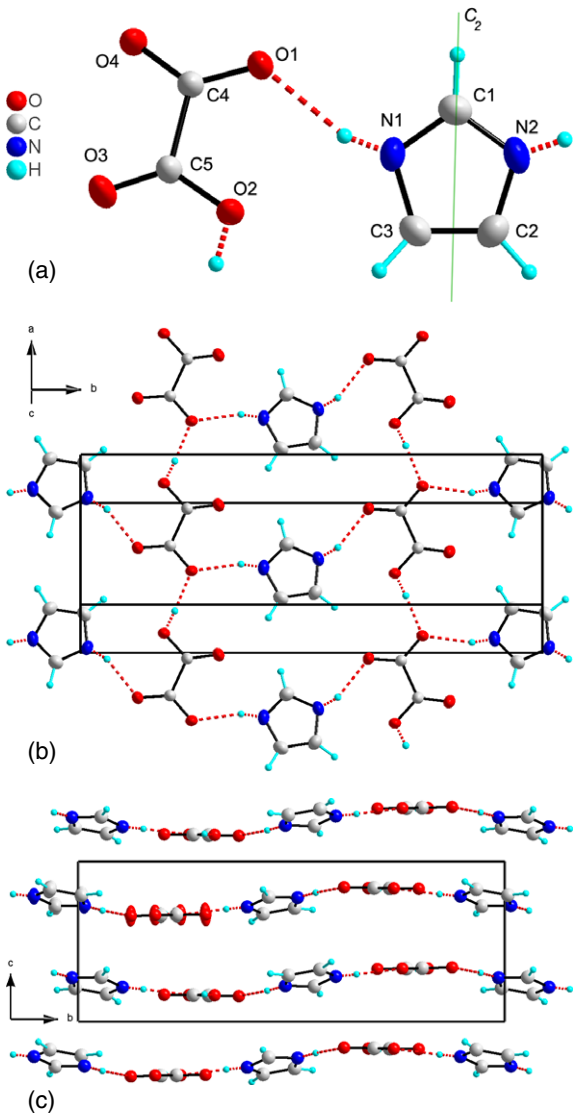

Figure 1. (a) A schematic diagram of the molecular structure of imidazolium oxalate: C_2, reorientation axis of the imidazole ring; C1, apical, and C2, C3, basal carbons of the ring. (b), (c) The hydrogen-bonded layers formed in imi-oxalate.

bonds to form chains composed of alternating imidazolium cations and carboxylic anions (motif A). The anions formed O–H $\cdots$ O hydrogen bonds in head-to-tail arrangements (motif B). Intersections of motifs A and B formed layers of molecules in the studied structure as shown in figure 1. The two-dimensional network of the hydrogen bonds in the layer is the characteristic future of the crystal structure of the imi-oxalate and allows for proton transport in the system.

3.2. Proton spin–lattice relaxation

^{1}H spin–lattice relaxation measurements allow us to directly probe protons as the nuclei responsible for conduction in the imi-oxalate. If the idea concerning ^{1}H conductivity in this material is correct then it should be reflected in the molecular mobility. It is considered that in imi-oxalate, as in other imidazole-based proton-conducting materials, the

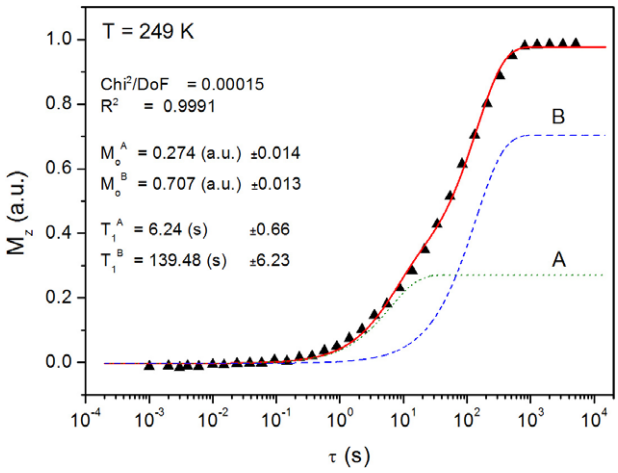

Figure 2. The time dependent recovery of the magnetization $M_z(\tau)$ measured for imi-oxalate at 249 K. The solid line is the best fit of the two parameter exponential function to the experimental points.

proton transport is a Grotthus mechanism. Thus, it is reasonable to assume that this cooperative process involves fast proton hopping between hydrogen-bonded imidazole rings and their thermally activated rearrangements. Saturation-recovery experiments yielding longitudinal or spin–lattice relaxation (T_1) times quantify not only the degree of molecular mobility but also the nature of the H-bonded domains.

In figure 2 the time dependent recovery of the magnetization $M_z(\tau)$ measured for imi-oxalate at 249 K is presented. A biexponential recovery of magnetization is clearly seen in the figure and was found within the whole range of the studied temperature. The experimental data were fitted with the help of two exponential functions:

$$M_z(\tau) = M_o^A[1 - \exp(-\tau/T_1^A)] + M_o^B[1 - \exp(-\tau/T_1^B)], \quad (1)$$

where T_1^A and T_1^B are the spin–lattice relaxation times and M_o^A and M_o^B are equilibrium values of the magnetization. The fitted procedure gave the values of two relaxation times for each studied temperature (T_1^A and T_1^B) and also the two components of magnetization (M_o^A and M_o^B). These parameters are presented in figures 3 and 4, respectively. The temperature dependences of the spin–lattice relaxation times evidence that the two types of protons, significantly different as to the spin–lattice relaxation values, can be distinguished in the imi-oxalate: the fast and the slow protons. The relaxation time T_1^A for mobile protons is of the order of about 10 s in the temperature range from 98 to 250 K. Above 250 K, far below the melting temperature of 523 K, a significant decrease of this component of relaxation is observed. The slow protons are characterized by the relaxation time T_1^B of about 200 s in the temperature range from 98 to 250 K. Above 250 K the shortening of this longer component of the relaxation is also observed but is not so well pronounced as in the case of the short T_1^A component. From figure 4 it is seen that the M_o^A magnetization associated with the short relaxation time T_1^A constitutes about 25% of the total magnetization and its contribution slightly increases with the increase of

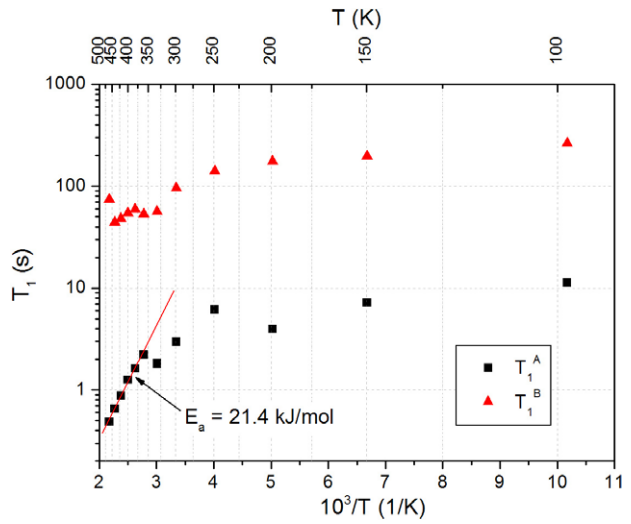

Figure 3. The two components of the proton spin–lattice relaxation times measured for imi-oxalate. The solid line is the best fit of the Arrhenius law to the experimental points of the short component of relaxation.

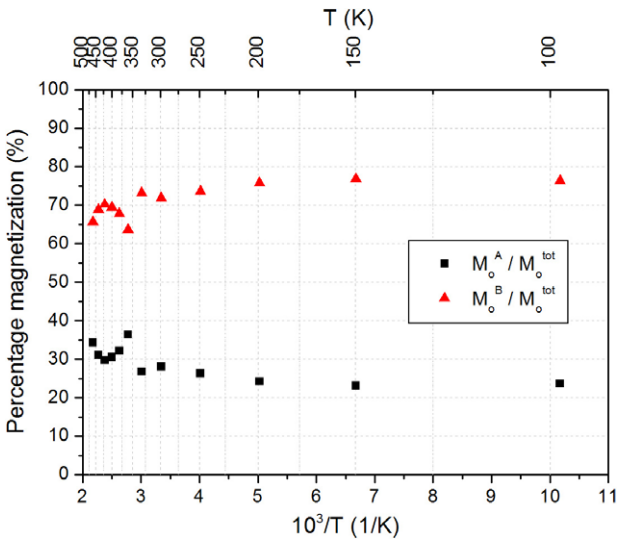

Figure 4. The two components of magnetization shown as a function of temperature. They correspond to the relaxation data presented in figure 3.

the temperature. At 450 K this participation is about 35%. Consequently, the magnetization M_o^B connected with the long relaxation time T_1^B determines the main part of the total magnetization measured in our experiment.

The high-resolution ^{1}H solid-state NMR methods have been widely used to study the proton dynamics in imidazole-based materials and imidazole itself [9, 11, 13, 16, 17]. These results clearly show that in the materials based on imidazole molecules two phases or two parts can always be distinguished before the glass transition or melting point, that is, the ordered (rigid) and disordered (mobile) phases. The ordered part is attributed to the rigid imidazole rings with a strong hydrogen bond whereas the disordered component to mobile rings with weak or dynamically averaged hydrogen bonds. It is interesting that only a small fraction of the imidazole-based material exists in the mobile state at 330 K (about 5–30%) [9, 11, 13, 16, 17].

Our proton spin–lattice relaxation measurements evidence, through the mobile and rigid protons, that also in the studied imi-oxalate there exist two dynamically different phases. The mobility of protons is associated and probably enhanced by the presence of a structural defect. The question arises as to the particular type of motion that can cause the significant reduction of the relaxation time above 250 K. The activation energy E_a calculated from the slope of the temperature dependence of the short component of T_1^A versus temperature is equal to 21.4 kJ mol^{-1}. We assumed that this is the energy for the imidazolium ring reorientation which takes place in the mobile part of the material. The ring-flip process has been well documented in the NMR experiments and also investigated by studying diffusion of an excess process in the imidazole chain using *ab initio* molecular dynamics simulation [13, 17, 21]. The imidazolium ring performs a 180°-flip motion around an axis parallel to the apical C–H bond (C_2 axis—see figure 1(a)). The activation energy for the imidazolium ring reorientation obtained for imi-oxalate is comparable to the values determined for other imidazole-based materials [13, 17]. Some differences can arise from the relative strengths of the interactions and the packing geometries of the materials. In imi-oxalate, the ring reorientation requires breaking and reforming of the hydrogen bonds whereas, e.g., in imidazolium methylsulfonate the energy is required to break the stronger electrostatic or Columbic interactions. This gave rise to the higher activation energy of 38.5 kJ mol^{-1} in this material. The spin–lattice relaxation measurements in the studied compound indicate that the reorientation of the imidazolium ring begins above 250 K. This is consistent with impedance spectroscopy measurements of macroscopic proton conduction in imidazole salts of dicarboxylic acids, in which an abrupt increase of the proton conductivity is observed above 260 K [2, 3].

The interpretation of our ^{1}H NMR relaxation measurements was based up until now on the results published for other imidazole-based proton conductors [9, 11, 13, 6, 17]. However, in the next paragraph we will give the experimental evidence of the imidazolium ring reorientation in imi-oxalate through the high-resolution solid-state NMR spectra.

We conclude that the proton spin–lattice relaxation time can be successfully used to evidence the protons that are mobile on the timescale of the experiment, and are able to participate in charge transport and also the reorientation of the imidazolium rings, important in proton transport mechanisms.

3.3. ^1H–^{13}C CP/MAS spectra

High-resolution solid-state NMR under fast magic spinning was used to study the structural dynamics in imi-oxalate. The studies were based on the cross-polarization transfer of magnetization from ^{1}H to ^{13}C, required for dipolar interactions to not be averaged out completely by the magic angle spinning of the sample. In general, the CP/MAS experiment is selected against any mobile carbons (protons) and thus dominated by

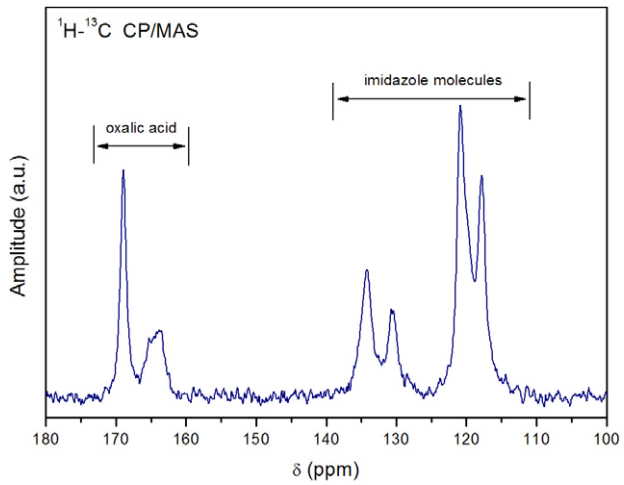

Figure 5. The ^{1}H–^{13}C CP/MAS NMR spectrum of imi-oxalate recorded with spinning at 8 kHz. The resonances below 140 ppm arise from imidazole molecules whereas peaks above 160 ppm are attributed to oxalic acid.

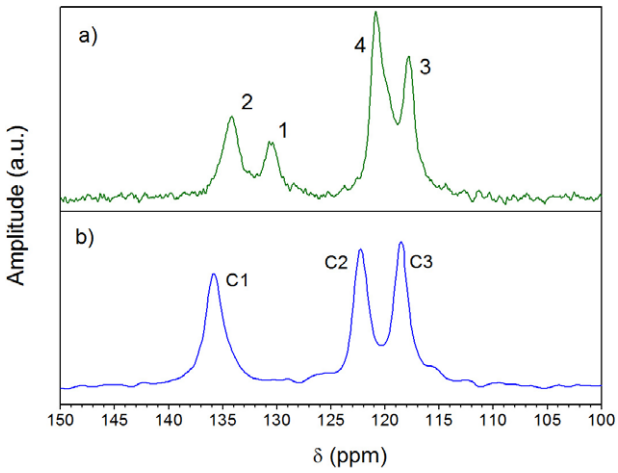

Figure 6. (a) The part of ^{1}H–^{13}C CP/MAS NMR spectrum of imi-oxalate assigned to the imidazole molecules; (b) typical spectrum taken for rigid imidazole molecules: C1—apical carbons, C2 and C3—basal carbons.

signals from rigid molecules. The dipolar interactions are reduced as a consequence of molecular motions and thus are weaker for mobile spins than for rigid spins. However, the spinning frequency of 8 kHz used in our experiment did not average out completely even the weaker dipolar interactions and thanks to this the mobile molecules also produce signals under cross-polarization.

The ^{1}H–^{13}C CP/MAS spectrum of imi-oxalate, recorded at room temperature with MAS at 8 kHz and the repetition time of about 10 s, is presented in figure 5. The resonances below 140 ppm arise from imidazole molecules whereas peaks above 160 ppm are attributed to oxalic acid. The part of the spectrum of interest for our discussion is the one in the range of 100–140 ppm assigned to imidazole molecules and redrawn in figure 6(a). For comparison the typical ^{1}H–^{13}C CP/MAS NMR spectrum for a rigid imidazole molecule is presented in figure 6(b). It contains three imidazole resonances: two peaks for basal carbons C3 and C2 (see figure 1(a)) at about 118 and 122 ppm, respectively, and one peak at about 136 ppm, assigned to apical carbon C1 [22]. In different imidazole-based materials the relative positions of the three imidazole resonances slightly differ due to the different hydrogen-bonding strengths in which imidazole molecules are involved in the particular materials. Thus, the resonances at 117.8 ppm, the next at 120.9 ppm, and the one at 134.5 ppm observed in the spectrum for imi-oxalate presented in figure 6(a) can be easily assigned to carbons of the rigid imidazole molecules. But what is the origin of the peak at 131 ppm and what causes the asymmetry of the resonance line observed for basal rigid carbon at 120.9 ppm?

In imidazolium methyl sulfonate, the material considered as a model system for new proton-conducting materials based on imidazole, a ring orientation about the C_2-axis of the ring (see figure 1(a)) is observed in the ^{1}H–^{13}C MAS spectrum and well documented [17]. The reorientation is evidenced through the coalescence process of basal ^{13}C resonances of imidazole molecules. The spectrum of imidazole molecules

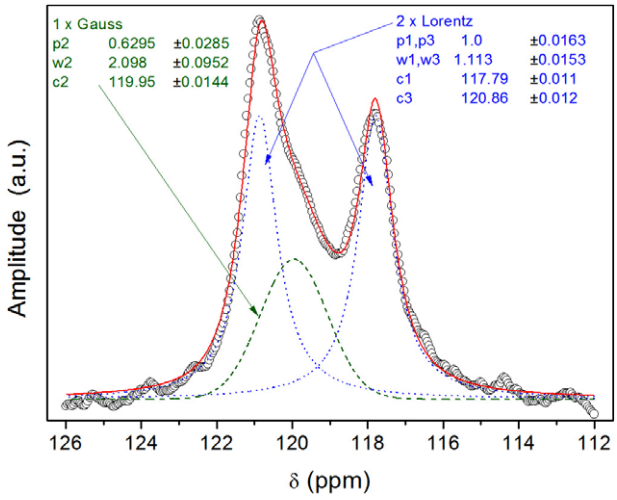

Figure 7. Part of the ^{1}H–^{13}C CP/MAS NMR spectrum of imi-oxalate, which presents only the resonances for basal carbons of the imidazolium molecules. Decomposition of the line showed two peaks at 117.8 and 120.9 ppm for rigid molecules and one coalescence line at 119.5 ppm for mobile molecules. The p, w and c symbols are the area (a.u.), width (ppm) and center (ppm) parameters of the fitted lines, respectively.

which undergo the ring reorientation consists only of two peaks: one for apical carbon (C1) and one for basal carbons (C2 and C3). The latter is the average resonance involving the resonances of the sites C2 and C3 in slow exchange. Only the motional processes which are slow with respect to the NMR timescale (on the millisecond timescale) can be detected via the coalescence phenomenon.

Therefore, we attributed the peak observed at 131 ppm in the spectrum from figure 6(a) to apical carbons of the mobile imidazole molecules. The line shape analysis of the resonances in the spectrum range from 112 to 126 ppm presented in figure 7 helps us find the resonance of basal carbons of mobile molecules at 119.9 ppm. The experimental spectrum was fitted

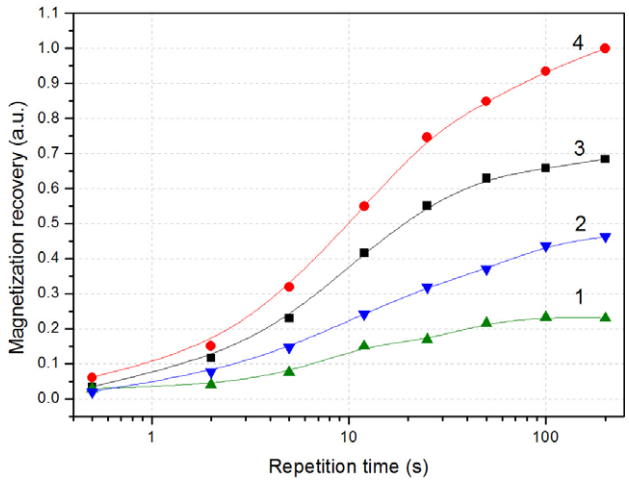

Figure 8. The recovery of the amplitude for the resonances observed in imi-oxalate spectra taken at room temperature as a function of the repetition time. Lines 3, 4 (basal carbons) and 2 (apical carbons) are assigned to rigid imidazole molecules whereas line 1 to the mobile molecule.

with the help of two Lorentzian lines (with the same area parameter) assumed for rigid imidazole molecules, and one Gaussian for the mobile molecules. All fitting parameters are shown in figure 7. The line width of the coalescence Gaussian is about 2.1 ppm, whereas the Lorentzian one is about 1.1 ppm. This suggests that the rate of the ring reorientation is close to that expected for the line coalescence. The line coalesces at the rate constant [23]

$$k_{\text{coalesc}} = \pi \Delta\upsilon/\sqrt{2} \tag{2}$$

where $\Delta\upsilon$ is the difference of the resonance frequencies. At this rate constant, the line width is at its maximum and the amplitude is at its minimum. For increasing rate, the single line becomes narrow again. In our experiment the temperature is the factor which determined the increasing of the rate constant. The analyzed spectrum was taken at room temperature and through the width of the mobile basal carbon resonance we can conclude that at this temperature the rate of imidazolium ring reorientation causes the coalescence phenomenon.

In figure 8 the recovery of the amplitude is presented for the resonances observed in imi-oxalate spectra taken at room temperature as a function of the repetition time. Lines 3, 4 (basal carbons) and 2 (apical carbons) are assigned to rigid imidazole molecules. Line 1 is for an apical mobile molecule. In this graph the basal line for the mobile molecule was not extracted from line 4. The recoveries of the amplitude were measured in the time range of 0.2–200 s and only for the line associated with the mobile molecules—apical carbon (line 1)—is the maximal amplitude of the line (full recovery of the magnetization) observed. The lines connected with the rigid molecules characterized by the long spin–lattice relaxation time do not fully recover in the studied period of time. This experimental finding proves our assignment of lines in the imi-oxalate spectrum of imidazole rings.

The interpretation of the ^{1}H–^{13}C CP/MAS spectrum of imi-oxalate gave additional evidence that the imidazolium salt of oxalic acids comprises a mixture of ordered and disordered components. The resonances at 117.8, 120.9 and 134.5 ppm are assigned to the rigid imidazole rings whereas the resonances at 119.9 and 131 ppm are assigned to imidazole rings undergoing reorientation. The evidence of the ring reorientation process which is found here to occur in imi-oxalate will provide deeper insight into one step in the proton transport in the imidazolium salts of dicarboxylic acids, of interest for fuel cells.

4. Conclusion

The present work essentially demonstrates the existence of two types of imidazole molecules in imi-oxalate below the melting point: mobile and rigid ones. They are evidenced by proton spin–lattice relaxation measurements and by the ^{1}H–^{13}C CP/MAS spectra of the studied compound. The mobile imidazole rings represent disordered domains, which are proposed to be responsible for the proton conductivity observed in the studied compound as well and in other imidazolium salts of dicarboxylic acids below the melting temperature. The disordered or mobile phase consists of about 35% of the sample at 400 K. The rigid imidazole rings represent the ordered domains and constitute the main part of the sample. In the ordered phase the imidazole rings are involved in a strong hydrogen bond whereas within the disordered domains the rings form a weak or dynamically averaged hydrogen bond which allows for proton transport via the Grotthus mechanism. Moreover, the observation of the coalescence phenomenon involving the resonances of the basal carbons of the imidazolium ring in ^{13}C CP/MAS NMR spectra of imi-oxalate provides evidence of the microscopic process, i.e. the reorientation of the imidazole ring. This gives rise to proton transport in the imidazolium oxalate material and, as such, this experimental finding provides important information for further development of material with potential applications for membranes in fuel cells.

The electrical conductivity measurements identify the proton conductors and measure the macroscopic conductivity but only advanced NMR methods can go inside the microscopic nature of the conductivity.

Despite good evidence of the mobile phase in all imidazole-based materials given by NMR measurements the origin of this phase is still not fully understood. It is most probably due to the presence of defects, grain boundaries or amorphous domains as in the crystalline imidazole [13].

Acknowledgments

The authors would like to thank Professor Marek J Potrzebowski from the Centre of Molecular and Macromolecular Studies, Polish Academy of Sciences, Łódź, Poland, in whose laboratory the CP/MAS measurements were performed, and Włodzimierz Ciesielski for his expert experimental assistance.

References

[1] MacDonald J C, Dorrestein P C and Pilley M M 2001 *Cryst. Growth Des.* **1** 29–38

[2] Pogorzelec-Glaser K, Garbarczyk J, Pawlaczyk Cz, Pietraszko A and Markiewicz E 2006 *Mater. Sci. Poland* **24** 245–53
[3] Pogorzelec-Glaser K, Pawlaczyk Cz, Pietraszko A and Markiewicz E 2007 *Power Sources* **173** 800–5
[4] Garbarczyk J and Pogorzelec-Glaser K 2003 *Z. Kristallogr.* **218** 567–8
[5] Kreuer K D 1997 *Solid State Ion.* **97** 1–15
[6] Kreuer K D, Dippel Th and Maier J 1995 *Membrane Materials for PEM-Fuel-Cells: a Microstructural Approach in Proton Conducting Membrane Fuel Cells I* vol PV 95-23, ed Sh Gottesfeld *et al* (Pennington, NJ: The Electrochemical Society) pp 241–6
[7] Kreuer K D, Fuchs A, Ise M, Spaeth M and Maier J 1998 *Electrochim. Acta* **43** 1281–8
[8] Kreuer K D 1998 New proton conducting polymers for fuel cell applications *Solid State Ionics: Science and Technology* ed B V R Chowdari (Singapore: World Scientific) pp 263–74
[9] Schuster M, Meyer W H, Wegner G, Herz H G, Ise M, Schuster M H D, Kreuer K D and Maier J 2001 *Solid State Ion.* **145** 85–92
[10] Herz H G, Kreuer K D, Maier J, Scharfenberger G, Schuster M F H and Meyer W H 2003 *Electrochim. Acta* **48** 2165–71
[11] Goward G R, Schuster M F H, Sebastiani D, Schnell L and Spieß H W 2002 *J. Phys. Chem.* B **106** 9322–34
[12] Schuster M F H, Meyer H W, Schuster M and Kreuer K D 2004 *Chem. Mater.* **16** 329–37
[13] Fischbach I, Spieß H W, Saalwachter K and Goward G R 2004 *J. Phys. Chem.* B **108** 18500–8
[14] Agmon N 1995 *Chem. Phys. Lett.* **244** 456–62
[15] Kreuer K D 1997 *Solid State Ion.* **94** 55–62
[16] Hickman B S, Mascal M, Titman J and Wood I G 1999 *J. Am. Chem. Soc.* **121** 11486–90
[17] Goward G R, Saalwachter K, Fischbach I and Spieß H W 2003 *Solid State Nucl. Magn. Reson.* **24** 150–62
[18] Sheldrick G M 1997 *SHELXS-97, Program for Solution of Crystal Structure Refinement* University of Götingen
[19] Petricek V, Dusek M and Palatinus L J 2000 *Structure Determination Software Programs* (Praha: Institute of Physics)
[20] Kuhs W F 1983 *Acta Crystallogr.* A **39** 148–58
[21] Munch M, Kreuer K D, Silvestri W, Maier J and Seifert G 2001 *Solis State Ion.* **145** 437–43
[22] Potrzebowski M J, Cypryk M, Michalska M, Koziol A E, Kazmierski S, Ciesielski W and Klinowski J 1998 *J. Phys. Chem.* B **102** 4488–94
[23] Spieß H W 1985 *Adv. Polym. Sci.* **66** 23–58